

RESEARCH ARTICLE | FEBRUARY 23 2024

## Outcomes from water drop impact on hydrophobic meshes



Raziyeh Akbari (راضیه اکبری) ; Yu Wei (魏瑀) ; Alberto Bagni ; Riccardo Ruffo ; Marie-Jean Thoraval (陶益壯) ; Longquan Chen (陈龙泉) ; Carlo Antonini



*Physics of Fluids* 36, 027137 (2024)

<https://doi.org/10.1063/5.0189860>

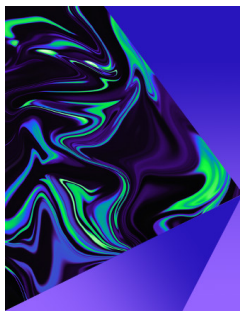


View  
Online



Export  
Citation

CrossMark



## Physics of Fluids

Special Topic:

Selected Papers from the 2023 Non-Newtonian  
Fluid Mechanics Symposium in China

**Submit Today**



# Outcomes from water drop impact on hydrophobic meshes

Cite as: Phys. Fluids **36**, 027137 (2024); doi: [10.1063/5.0189860](https://doi.org/10.1063/5.0189860)

Submitted: 1 December 2023 · Accepted: 29 January 2024 ·

Published Online: 23 February 2024







View Online



Export Citation



CrossMark

Raziyeh Akbari (راضیه اکبری),<sup>1,a)</sup>  Yu Wei (魏瑀),<sup>1,2</sup>  Alberto Bagni,<sup>1</sup>  Riccardo Ruffo,<sup>1</sup>   
Marie-Jean Thoraval (陶益壯),<sup>2,3</sup>  Longquan Chen (陈龙泉),<sup>4,5</sup>  and Carlo Antonini,<sup>1,a)</sup> 

## AFFILIATIONS

<sup>1</sup>Department of Materials Science, University of Milano-Bicocca, via R. Cozzi 55, 20125 Milano, Italy

<sup>2</sup>School of Aerospace, Xi'an Jiaotong University, Xi'an 710049, People's Republic of China

<sup>3</sup>Laboratoire d'Hydrodynamique (LadHyX), CNRS, École Polytechnique, Institut Polytechnique de Paris, 91120 Palaiseau, France

<sup>4</sup>School of Physics, University of Electronic Science and Technology of China, Chengdu 610054, People's Republic of China

<sup>5</sup>Institute of Electronic and Information Engineering of UESTC in Guangdong, Dongguan 523808, People's Republic of China

<sup>a)</sup> Authors to whom correspondence should be addressed: [raziyeh.akbari@unimib.it](mailto:raziyeh.akbari@unimib.it) and [carlo.antonini@unimib.it](mailto:carlo.antonini@unimib.it)

## ABSTRACT

Understanding water drop impact on meshes is valuable to design passive systems for atmospheric water collection. By investigating water drop impact on hydrophobic and superhydrophobic surfaces, here, we identify the different drop impact outcomes and build outcome maps within the pertinent parameter spaces, based on Weber number and contact angles. Furthermore, we quantitatively evaluate critical factors such as the captured volume and spray characteristics of the penetrating liquid and also measure the drop rebound time, reporting that full rebound occurs on superhydrophobic meshes surfaces even at high We numbers, as the Cassie–Baxter wetting state is maintained.

Published under an exclusive license by AIP Publishing. <https://doi.org/10.1063/5.0189860>

## I. INTRODUCTION

Water harvesting from atmospheric fog is a passive low-technology route to collect water in areas threatened by drought, offering a cost-effective alternative to energy-intensive processes like desalination with  $\sim 3 \text{ kWh m}^{-3}$  energy cost.<sup>1</sup> Recently, water harvesting using meshes has attracted increasing interest because of its high efficiency in water harvesting and directional transportation.<sup>2–6</sup> To understand the optimal conditions for maximizing water harvesting efficiency, fundamental studies of water single drop impact on a mesh are required.

Drop impact is a complex event governed by inertial, capillary, and viscous forces, as captured by the typical non-dimensional numbers, such as the Weber number  $We = \rho D_0 U^2 / \sigma$ , the Ohnesorge number  $Oh = \mu / \sqrt{\rho \sigma D_0}$ , and their combination, the Reynolds number,  $Re = \sqrt{We} / Oh$ ;  $\rho$ ,  $\sigma$ ,  $\mu$ ,  $U$ , and  $D_0$  are the drop density, surface tension, viscosity, impact velocity, and diameter, respectively. Spreading, recoiling, jetting, splashing, breaking up, and rebounding are possible drop impact outcomes on solid flat surfaces.<sup>7–13</sup> The complexity increases in drop impact on porous materials, such as meshes with sub-millimetric pores as water can be trapped within the pores and penetrate through the mesh eventually breaking into many smaller drops.<sup>14</sup> By tuning the  $We$  number, outcomes including imbibition,

penetration, fragmentation, and spray can be observed during drop impact on a mesh.<sup>15–19</sup>

In the impact of a millimetric drop, characteristic pore sizes are typically classified as large ( $\sim$ some hundreds of  $\mu\text{m}$ ),<sup>20–22</sup> moderate ( $\sim 100 \mu\text{m}$ ),<sup>16,23</sup> and small ( $\sim 10 \mu\text{m}$ ),<sup>24</sup> where the drop impact outcomes are a function of the ratio between the drop diameter and the surface pore size.<sup>20,25</sup> Wetting properties also play a non-negligible role in defining the drop impact outcomes and liquid dynamics, particularly in the recoiling and penetration through meshes.<sup>26–28</sup> Ryu *et al.*<sup>27</sup> demonstrated that while on regular meshes, liquid penetration occurs during the impact initial stages on superhydrophobic meshes, and penetration can also occur during recoil due to the energy accumulation in the drop just prior to recoil. This event was confirmed by Mehrizi *et al.*<sup>29,30</sup> with viscoelastic drops impacting on superhydrophobic meshes and by Sen *et al.*<sup>31</sup> in the drop impact experiments on step wettability-patterned metal meshes. However, by changing the common orthogonal configuration to the inclined experimental setup, the penetration related outcomes could be occurring at larger  $We$  numbers depending on the inclination angle, as studied by Xu *et al.*<sup>32</sup> The drop contact time with the surface is also one of the main differences between the flat surface and the highly porous samples like meshes. While the previous studies such as Richard *et al.*<sup>33</sup> showed

that the contact time is almost constant and independent of the impacting velocity on the flat surfaces, studies on the porous surfaces, especially meshes, revealed that after a critical drop impacting velocity, the contact time decreases by increasing  $We$ , due to the increase in the drop penetration into the pores and breakdown.<sup>21,34,35</sup> In addition, Song *et al.*<sup>34</sup> investigated the stability of hydrophobicity in the coated mesh by drop impact experiments at various impact conditions.

It is worth mentioning that various simulations and numerical models have been developed and used to interpret drop impact results and help to establish a theoretical framework, revealing new insights not easily captured in experiments due to limitations.<sup>31,36–38</sup> Specifically, the velocity distribution, internal hydrodynamics in the drop, and the energy evolution are accessible only in the simulation, enabling a more complete understanding of the postimpact outcomes in complex surface morphologies and in multi-phase flows. For instance, Catsoulis *et al.*<sup>36</sup> introduced a three-dimensional computational framework, improving the volume-of-fluid (VOF) method, to analyze drop impact on patterned surfaces. Their findings emphasize on the crucial role of wettability contrast and contact angle hysteresis in drop dynamics on meshes. Additionally, Wang *et al.*<sup>37</sup> explored the influence of surface tension and viscosity of the liquid on drop outcomes on meshes using lattice Boltzmann (LB) simulation. However, while the simulation methods have limitations in the dimensions of the simulated system and the accuracy of the implemented dynamics due to the computational costs, it is crucial to assess the relevance of the results by comparing them with experimental findings.

The present study investigates the effect of mesh wettability, tuned by growing microstructures on mesh wires, on the characteristic drop impact outcomes and the impact outcome map in the relevant parameter spaces as well as quantitatively assess captured drop volume, the drop rebound time (in the case of rebound occurs), and the spray characteristics of the penetrating liquid. The wider objective is to define design principles for the fabrication of atmospheric water harvesters using meshes.

## II. EXPERIMENTAL METHODS

A copper (Cu) layer is electrodeposited on #185 stainless steel meshes (S0, reference uncoated sample, opening  $l = 80 \mu\text{m}$ , wire diameter  $w = 50 \mu\text{m}$ , and sample size =  $2.5 \times 1.5 \times 0.005 \text{ cm}^3$ ) in the cyclic voltammetry mode for 1–3 cycles (S1–S3 samples, respectively).<sup>39–41</sup> S4 was produced following the same electrodeposition process as S3, adding a monolayer of 1H, 1H, 2H, and 2H-perfluorododecyltrichlorosilane (FTS).<sup>42</sup> Electrodeposition was performed using aqueous 0.1 M  $\text{CuSO}_4$  as electrolyte, and Pt wire and saturated calomel electrode (SCE) as counter and reference electrodes, respectively. The potential was swept between 0 (vs ref) and  $-1.2 \text{ V}$  with a scan rate of  $20 \text{ mV s}^{-1}$ . For hydrophobization of S4, the sample was immersed in 2.2 mM FTS solution in hexane for 1 minute and rinsed in hexane afterward. In drop impact tests with distilled water ( $\rho = 997 \text{ kg/m}^3$ ,  $\sigma = 72.8 \text{ mN/m}$ , and  $\mu = 1.0016 \text{ mPa s}$ , at room temperature<sup>43</sup>), the drop diameter was  $D_0 = 2.06 \pm 0.01 \text{ mm}$  ( $\sim 4.6 \mu\text{l}$ ), and impact velocities were  $U = [0.4, 3.2] \text{ m s}^{-1}$ , corresponding to  $We = [4, 292]$ . Here, both  $D_0$  and  $U$  measured from the experiment videos, see the discussion on the uncertainty analysis in the supplementary material. Note that the range of  $We$  for millimetric drops impacting on a mesh investigated here is comparable to the case of 50–100  $\mu\text{m}$  fog droplets impacting on meshes after being transported by wind with velocities of  $\sim 15\text{--}25 \text{ m s}^{-1}$ . The impact was captured using a high-speed camera (Photron Fastcam SA4)

with a spatial resolution of  $20 \mu\text{m px}^{-1}$  and a frame rate of 5 kfps with backlight illumination [see a schematic of the setup in Fig. 1(a)]. The same optical setup was used to measure the wetting characteristics, advancing ( $\theta_a$ ) and receding ( $\theta_r$ ) contact angles, and, consequently, wetting hysteresis ( $\Delta\theta$ ). All wettability test results were analyzed by Dropen software.<sup>44</sup> All wetting and impact measurements were repeated at least three times to ensure reproducibility. The information was complemented by morphology analysis using a scanning electron microscope (SEM, Vega TS5136 XM, TESCAN).

The surface morphology and wetting characteristics of S0–S4 are presented in Figs. 1(b)–1(f). By increasing the copper deposition cycles from 1 to 3 (S1 to S3), dendritic rough structures grow on the mesh wires, enhancing hydrophobicity with  $\theta_a$  and  $\theta_r$  up to  $160^\circ$  and  $138^\circ$ , respectively, and reducing contact angle hysteresis  $\Delta\theta$  down to  $22^\circ$ . The additional hydrophobization using the silane, providing a conformal coating (S4), leads to an increase in the receding contact angle  $\theta_r = 148^\circ$ , and a lower hysteresis  $\Delta\theta = 9^\circ$  and made the sample superhydrophobic.<sup>45–47</sup>

## III. RESULTS

Examples of the impact sequences by increasing  $We$  are presented in Fig. S1 in the supplementary material. At low  $We$  ( $< 30$ ), the impact is characterized by a spreading phase, followed by recoil and the formation of a vertical Worthington jet and eventually satellite drop ejection from the pinnacle apex, similar to the impact on a solid non-porous surface. By increasing  $We$  ( $> 30$ ), water imbibes the mesh: this leads to liquid penetration with a visible bulge on the bottom side, eventually followed by drop fragmentation and then followed by a

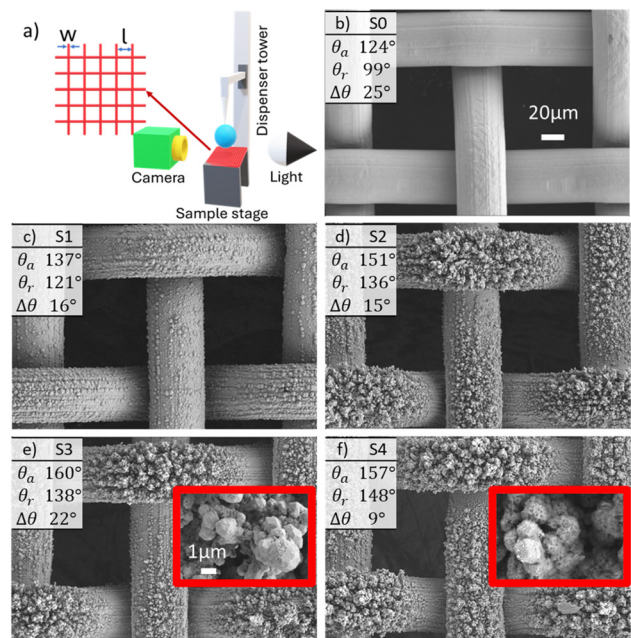


**FIG. 1.** (a) A schematic of the home-made drop impact test setup with the indication of dimensions of the mesh. (b)–(f) SEM images along with the wetting characteristics of S0–S4 samples. Insets in e and f are magnified images of the surfaces before (S3) and after (S4) silanization. The error in the contact angle measurements is  $< \pm 3^\circ$ .

recoil above the mesh. At even higher  $We$  ( $\sim 150$ ), the liquid penetrating the mesh is fragmented into a spray distributed in a cone under the mesh. In the meantime, the liquid held on the mesh top side can first spread and then recoil: the higher the hydrophobicity, the higher the recoil. In the case of superhydrophobic surfaces, the rebound is promoted.

Figures 2(a)–2(d) (Multimedia view) illustrate the main drop impact outcomes above the mesh. Qualitatively, and four different outcomes are observed: deposition and column formation (DE), column formation with drop ejection (CD), partial rebound (PR), and full rebound (FR). The outcome map in Fig. 2(e) is represented in the  $(We, \theta_r)$  parameter space;  $\theta_r$  was selected as this is the relevant  $\theta$  value controlling the recoiling phase. On the least hydrophobic sample, S0, the dominating outcome is deposition. By increasing  $\theta_r$  (for S1, S2, and S3), the recoiling of the drop is enhanced, leading to a drop ejection at low  $We$  and deposition at high  $We$ . Also, for these samples, a few partial rebounds (PR) at low  $We$  ( $<20$ ) are observed. Full rebound is consistently observed on the superhydrophobic sample, S4, in the entire investigated  $We$  range. This is interesting, if compared to solid porous surfaces. Specifically, for pillar micropatterned surfaces with pillar spacing  $10\text{--}100\ \mu\text{m}$ , a transition from Cassie–Baxter to Wenzel state is expected in the Weber range investigated here: the liquid meniscus penetrated in the pores between the pillars and completely wet the pillar side, down to the bottom of the pore. The transition on non-porous surfaces is macroscopically manifested by pinning of the contact line, so that the drop cannot complete recoil, and full rebound is suppressed.<sup>48–53</sup> The transition does not seem to be relevant for a superhydrophobic mesh: indeed, even at a high  $We$  number, the liquid can imbibe the mesh and eventually penetrate the bottom side of the mesh, but the liquid remaining on the top side maintains a Cassie–Baxter wetting state, so that rebound can still occur on the superhydrophobic surface, S4, even in very high  $We$ . Drop receding breakup is also observed for samples S2 ( $We > 190$ ), S3 ( $We > 170$ ), and S4 ( $We > 150$ ): the critical threshold, thus, decreases with increasing contact angle, as highlighted by the dashed purple line in Fig. 2(e). Also, the number of satellite drops increases by increasing  $We$ , and their size distribution gets more uneven, as discussed in the literature.<sup>48,54</sup>

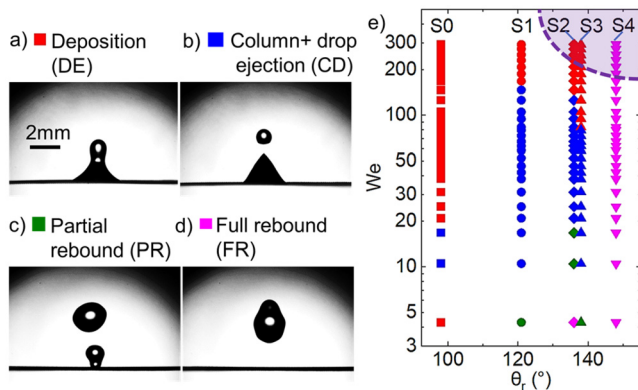


FIG. 2. (a)–(d) Images from different drop outcomes observed above the meshes (Multimedia available online). (e) A map of the observed phenomena above the mesh by increasing  $We$  and  $\theta_r$ . The dashed line and purple area correspond to the receding breakup region during recoiling in high  $We$ . Multimedia available online.

Figure 3 illustrates the drop impact outcomes focusing on the liquid dynamics below the mesh, with the outcome map represented in this case in the  $(We, \theta_a)$ , because  $\theta_a$  is relevant in the initial phase of mesh wetting. Qualitatively, five different outcomes are observed: no liquid penetration (NP), penetration without liquid detachment (PE), penetration with drop separation by breaking down (PSE), partial spray (PS), and full spray (FS), see Figs. 3(a)–3(e) for representative images. In NP, no liquid is visible below the mesh. In PE, a liquid bulge forms after impact below the mesh, but no liquid detaches; differently, in PSE, a small drop detaches.

From the penetration phase map in Fig. 3(f), the minimum  $We$  to observe a transition from no liquid penetration to penetration (either PE or PSE) is  $We_p \sim 30$ . This threshold is independent of wetting, which means that it mainly depends on the mesh pore size.<sup>27</sup> By further increasing the Weber number, a transition from penetration phases (PE or PSE) to partial and full spray (PS and FS, respectively) is observed, for  $We_s \sim 60\text{--}150$ , with a mild dependence on the contact angle: the threshold decreases by increasing  $\theta_a$ . A simple scaling confirms why transition occurs in this  $We$  range. Assuming that liquid penetration through the mesh is controlled by the balance between dynamic,  $P_D \sim (1/2)\rho U^2$ , and capillary,  $P_{Cap} \sim -2\sigma \cos \theta_a / r_C$ , pressures, where the characteristic length  $r_C$  can be considered roughly as half of the mesh opening  $l$ .<sup>15,27,55–58</sup> Thus, by neglecting viscous effects ( $Oh \ll 1$ ), the resulting critical Weber number is  $We < 8D_0/l = 206$ , as discussed earlier by Lorenceau *et al.*<sup>15</sup> and Soto *et al.*<sup>17</sup> However, results show that penetration starts at lower values. Indeed, the local liquid velocity has to be corrected to account for area restriction as the water flow passes through the pores. By simple math, the local velocity in the pore is  $U_p = ((l+w)/l)^2 U$ . Rewriting the dynamic pressure term as  $P_D \sim (1/2)\rho U_p^2$ , the critical  $We$  for the liquid penetration is  $We_p \sim (8D_0/l)(l/(l+w))^4 = 30$ , comparable to the experimentally observed  $We_p \sim 30$ .

Xu *et al.*<sup>59</sup> suggested a modified  $We$  as  $We/\cos \theta_a$ , to account for surface wetting properties. Mapping the drop impact outcomes vs

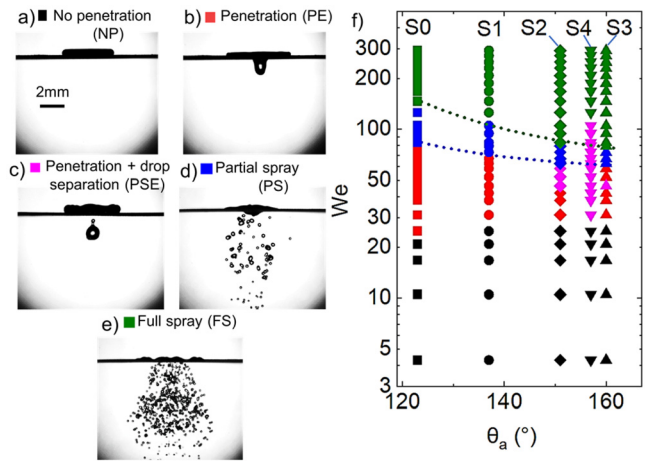


FIG. 3. (a)–(e) Images from different drop impact outcomes observed under the meshes. (f) A map of the drop impact outcomes under the mesh for samples with different advancing angles by increasing  $We$ . Dotted blue and green lines correspond to the fitting of critical  $We$  for the transition from PE to PS, and PS to FS, respectively, as a function of  $\theta_a$ , i.e.,  $-We/\cos \theta_a$ .



$We/\cos\theta_a$  can anticipate the critical impacting velocities and partially explain the earlier penetration in superhydrophobic meshes compared to hydrophobic ones. In the present study, tracking the transition from PE to PS and PS to FS in S0–S3 confirms this trend in critical  $We$  with  $1/\cos\theta_a$  in both the transitions [blue and green dotted lines in Fig. 3(f), correspondingly], and not occurs in the transition from NP to PE.

Figure 4(a) displays the dimensionless volume of liquid breakdown under the mesh,  $V_S/V_0$ , relative to the initial drop volume  $V_0$ , as a function of  $We$ :  $V_S/V_0=0$  corresponds to no liquid breaking down through the mesh, and  $V_S/V_0=1$  to full liquid breakdown. For  $We < We_S$ ,  $V_S$  is measured directly as the liquid penetrating and detaching under the mesh, while for  $We > We_S$ , where full spray develops,  $V_S$  is indirectly calculated as  $V_0$  minus the final volume on the mesh,  $V_D$ . For the superhydrophobic sample S4, with full rebound,  $V_S = V_0 - V_R$ , where  $V_R$  is the volume of the bounding liquid. In treated samples (S1–S4), drop breakdown begins at  $We > We_p$  and slightly increases afterward. In the un-treated sample, S0, there is a sharper rise in  $V_S$  after the starting of spray shower,  $We_S$ , due to lower surface tension and smoother wire surfaces, leading to less capillary anti-pressure and increased drop imbibition into the mesh.  $V_S$  increases by increasing  $We$  and decreasing the mesh hydrophobicity, i.e., liquid penetrates less on a superhydrophobic mesh. This is due to: 1. In a higher drop velocity, the drop dynamic pressure is much higher than the capillary anti-pressure in pores, as such, the increase in  $V_S$  is proportional to

$U^2$ , i.e., to  $We$ ; 2. A higher hydrophobicity requires overcoming a higher capillary anti-pressure, promoting the recoil phase. The increase in  $V_S$  in  $We > We_S$  can be assigned to a linear function of  $We$ , as presented in Fig. 4(a) by  $\zeta$ , with a slight change when transitioning from hydrophobic to superhydrophobic meshes. The amount of penetrating liquid also affects the drop spreading on the mesh top side. As presented in Fig. S2 in the supplementary material, the break time reduces quickly by increasing  $We$ , and in all the samples, the spray shower begins immediately after drop impact at  $We > We_S$ .

Figure 4(b) illustrates changes in the spray half-cone angle,  $\alpha$ , under the mesh as  $We - We_S$  increases.  $\alpha$  determined by the ratio of transversal and normal drop velocities passing through mesh pores,  $U_r$  and  $U_z$ , respectively, represented as  $\tan\alpha = U_r/U_z$ . In Fig. 4(b),  $\alpha$  increases by increasing  $We$  but decreases with greater surface hydrophobicity. The maximum  $\alpha$  drops from  $25^\circ$  in the less hydrophobic sample, S0, to  $6^\circ$  in the superhydrophobic sample, S4. The  $\tan\alpha$  trend follows a power of  $We - We_S$ ,  $\beta$ , with the power decreasing as mesh hydrophobicity increases. This can be attributed to the higher capillary anti-pressure in more hydrophobic samples. In a large  $We$  ( $We > 150$  or  $We - We_S \approx 0$ ), drops exceed the critical limit for passing through the mesh and form a spray shower, with higher capillary pressure increasing the speed of tiny droplets, as Vontas *et al.* show in Fig. 11 in Ref. 28. Additionally, larger  $\theta_r$  enhances the drop repellency from mesh pores, resulting in smaller  $\alpha$  for higher hydrophobicity. To understand the impact of spray volume on drop dynamics during impacting the mesh, a measurement of filled pores by penetrating and spraying liquid,  $D_t$ , is essential. Figure 5(a) shows changes in  $D_t$  during the full spray phase for two samples: less hydrophobic S0 and superhydrophobic S4. As sketched in the inset image in Fig. 5(a),  $D_t$  is measured as the diameter of the upper neck of the spray cone under the mesh. Accordingly,  $D_t$  increases with  $We$ , and overall coverage is lower in the superhydrophobic sample S4 compared to the reference S0, indicating less dissipation through mesh pores in the superhydrophobic sample. As discussed under Fig. 3, the liquid velocity in the pore channel increases by a factor of 2 for the tested meshes due to mass conservation. Soto *et al.*<sup>17</sup> demonstrated that increasing  $We$  leads to an increase in the half-cone angle and the mass transferred. However, this growth significantly reduces after reaching a critical  $\alpha$ , which is related to pore size and depth, similar to Fig. 4(b). Liwei *et al.*<sup>60</sup> also confirmed, both theoretically and experimentally, that the increase in  $\alpha$  by increasing  $We$  saturates in larger  $We$  ( $We > 300$  in their study), which is recently confirmed by Su *et al.*<sup>61</sup> in meshes with openings of 1 mm in width. Importantly, previous findings indicate that mesh wettability does not significantly influence the cone angle in large  $We$ , differently from our results shown in Fig. 4(b).

Figure 5(b) depicts the maximum non-dimensional spreading diameter,  $D_{max}/D_0$ , as a function of  $We$ , with a noticeable transition at  $We_p \approx 30$ . For  $We < We_p$ ,  $D_{max}$  scales as  $D_{max}/D_0 \propto W^a$ , with  $a = 0.22$ . This value aligns with other literature findings, such as Clanet *et al.*,<sup>62</sup> who proposed  $a = 0.25$ , and various studies<sup>9,63–65</sup> with values ranging from 0.20 to 0.50 (see Ref. 64 for a detailed comparison between experimental correlations, energy-based models, and hydrodynamic models). However, for  $We > We_p$ , different trends are observed, with  $a$  spanning from 0.19 for the superhydrophobic mesh (S4) to 0.08 for S0. This reveals two key distinctions between the drop impact on solid surfaces and meshes. First, on solid surfaces, wetting affects maximum spreading at low and moderate  $We$  ( $\sim 10^2$ ),<sup>64</sup> but at

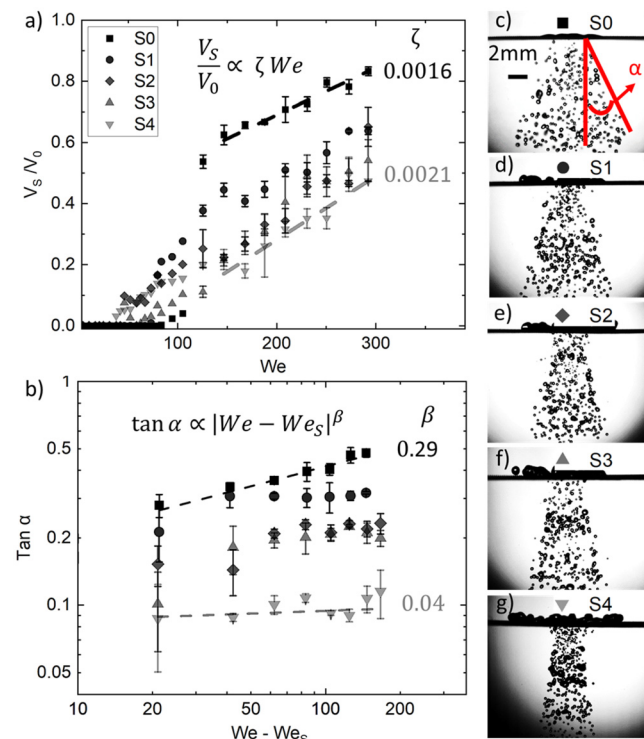
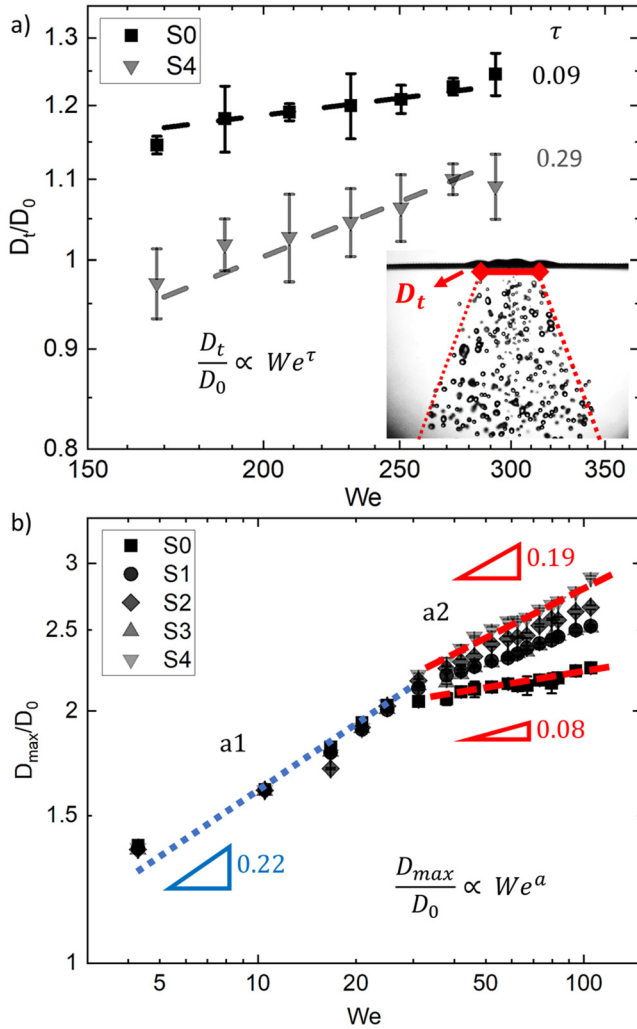
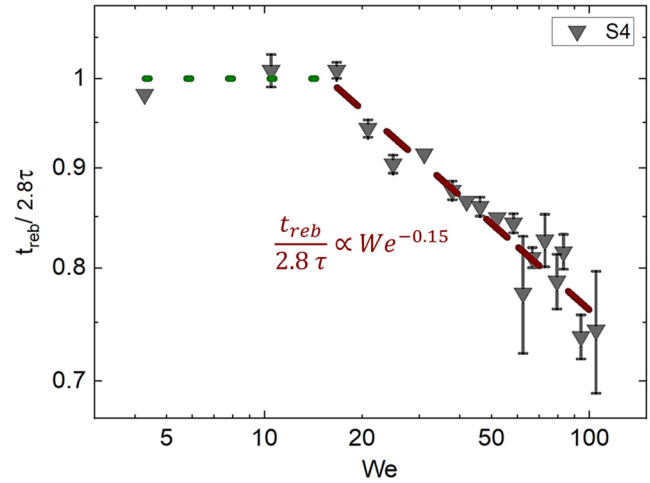


FIG. 4. (a) Spray volume and (b) spray half-cone angle vs  $We$  for different samples. (c)–(g) Images of the drop spray half-cone angle at  $We = 209$ . Lines show the fitting of the data to the written equation in the graphs.  $We_S$  is the full spray critical  $We$ , which is  $\sim [125, 147]$ , depending on the hydrophobicity.



**FIG. 5.** (a) The increase in the non-dimensional pore coverage by passing liquid through the mesh ( $D_t/D_0$ ) vs  $We$  in S0 and S4.  $D_t$  is graphically represented in the inset image. Dashed gray lines show fitting to the written equation in the figure. (b) The dimensionless drop maximum diameter during spreading above the mesh ( $D_{max}/D_0$ ) vs  $We$ . a1 and a2 are slopes for  $We < We_p$  ( $\sim 30$ ) and  $We > We_p$  ( $\sim 40$ ), respectively. Lines are proportional to the fitting equations written in the graph.

high  $We$ , where inertial forces dominate over capillary forces, wetting becomes negligible, and maximum spreading is solely dependent on  $We$ . In contrast, on meshes, wetting influences maximum spreading even at high  $We$ . Specifically, and here comes the second observation, maximum  $D_{max}/D_0$  is achieved on the superhydrophobic sample, S4, which may appear counterintuitive, given that drops typically spread less on more hydrophobic solid surfaces. However, this behavior can be explained by considering liquid penetration: on S4, liquid penetration is minimal, allowing more liquid to remain on the top side of the mesh and contribute to spreading. On less hydrophobic samples like S0, more liquid penetrates, resulting in less effective spreading liquid and reduced spreading. Thus, as shown in Fig. S3 in the supplementary



**FIG. 6.** The ratio between the drop rebound time and Rayleigh time in S4 vs  $We$ . The dotted green line shows the constant rebound time in  $We < 20$ , and the brown dashed line corresponds to the fitting equation presented in the graph.

material, modifying the initial drop diameter by considering  $V_S$  can alter the slope in S4 to slope in  $We < We_p$  but has no effect on the slope in S0.

Another classical parameter to investigate is the rebound time (also known as contact time), which is presented in Fig. 6 as a function of  $We$  for the superhydrophobic mesh, on which full rebound is observed. At low Weber numbers,  $We < 20$ , when the drop remains intact and no penetration occurs, the rebound time remains constant and equals  $t_{reb} = 2.8\sqrt{\rho D_0^3/8\sigma}$ . It is well known, since the observations of Wachters and Westerlings in the Leidenfrost regime, that the rebound time scales with the Rayleigh time  $\tau = \sqrt{\rho D_0^3/8\sigma}$ .<sup>55,63</sup> In previous studies on superhydrophobic and sublimating surfaces,<sup>63,64</sup> the pre-factor 2.6 was provided from the best fit of experimental data, which is comparable with the value 2.8 ( $\pm 0.2$ ) identified here for porous meshes. For  $We > 20$ , the rebound time decreases as  $t_{reb}/\tau \propto We^{-0.15}$ , resulting in a 25% reduction in  $t_{reb}$  at  $We = 106.33$ .<sup>66</sup> This decline can be attributed to mass loss of the main drop, which is, in principle, due to two separate phenomena: (i) drop fragmentation and separation from the main body during rebound due to receding breakup, as seen on non-porous superhydrophobic surfaces, and (ii) liquid penetration and breakdown through the mesh, for example, see Fig. 3 in Ref. 21 and Fig. 9 in Ref. 34. Based on the scaling  $t_{reb} \propto D^{3/2}$  mentioned earlier, the volume loss due to penetration [see Fig. 4(a)] contributes to a 10% reduction in rebound time at  $We < 106$ , see Fig. S4(a) in the supplementary material. This suggests that both mechanisms of mass loss (breakup and breakdown through the mesh) play a role. Additional information, including non-dimensional diameter evolution during rebound at various  $We$  numbers, is also available in Fig. S4(b) in the supplementary material. Calculations of retraction velocity confirm that liquid retracts and rebounds faster at higher  $We$ .<sup>54</sup>

#### IV. CONCLUSION

In this study, copper layers were deposited on stainless steel meshes. One of the samples was additionally coated with FTS to

increase its hydrophobicity. The investigation aims to understand the impact of surface wettability on the outcomes of the drop impact on hydrophobic meshes. Accordingly, water penetration through mesh is mainly affected by mesh structure,  $We_p \sim 30$ , while wettability matters more at higher  $We$ . Below  $We_p$ , drop spreading diameter scales with  $We^{0.22}$  regardless of wettability. However, beyond  $We_p$ , less hydrophobic surfaces show smaller increases in spreading diameter. A complete rebound occurs only in superhydrophobic silanized mesh ( $\Delta\theta < 10^\circ$ ) with rebound time as  $t_{reb} = 2.8\sqrt{\rho D_0^3/8\sigma}$  at  $We < 20$ . Rebound time decreases at higher  $We$  due to volume loss under the mesh, indicating Cassie–Baxter wetting. Critical  $We$  for drop breakdown and spray development scale with  $-1/\cos\theta_a$ . Higher hydrophobicity reduces the liquid kinetic energy dissipation during passing through the mesh, resulting in less spray volume and cone angle in hydrophobic samples. In conclusion, optimizing drop collection via the mesh involves avoiding both imbibition and full rebound, recommending highly hydrophobic meshes like S2 and S3 with  $\theta_r > 135^\circ$  and  $\Delta\theta < 25^\circ$ , respectively. Future research may explore coupling hydrophobic meshes with hydrophilic layers to reduce re-entrainment and blockage.

## SUPPLEMENTARY MATERIAL

See the supplementary material for insights into additional test results on drop spreading, rebound, and penetration dynamics.

## ACKNOWLEDGMENTS

R.A. and C.A. gratefully acknowledge support through a post-doctoral fellowship from the University of Milano-Bicocca, Italy. Y. W. and M.-J.T. received financial support from the National Natural Science Foundation of China (Grant No. 12072258). Y.W. acknowledges the financial support from China Scholarship Council (CSC).

## AUTHOR DECLARATIONS

### Conflict of Interest

The authors have no conflicts to disclose.

### Author Contributions

**Raziyeh Akbari:** Data curation (equal); Formal analysis (equal); Funding acquisition (equal); Investigation (equal); Methodology (equal); Visualization (equal); Writing – original draft (equal); Writing – review & editing (equal). **Yu Wei:** Data curation (equal); Formal analysis (equal). **Alberto Bagni:** Data curation (supporting). **Riccardo Ruffo:** Writing – review & editing (supporting). **Marie-Jean Thoraval:** Writing – review & editing (supporting). **Longquan Chen:** Writing – review & editing (supporting). **Carlo Antonini:** Conceptualization (equal); Funding acquisition (equal); Investigation (equal); Supervision (equal); Writing – review & editing (equal).

## DATA AVAILABILITY

The data that support the findings of this study are available within the article and its supplementary material.

## REFERENCES

- Y. Ghalavand, M. S. Hatampour, and A. Rahimi, “A review on energy consumption of desalination processes,” *Desalin. Water Treat.* **54**(6), 1526–1541 (2015).
- M. Cao, J. Xiao, C. Yu, K. Li, and L. Jiang, “Hydrophobic/hydrophilic cooperative Janus system for enhancement of fog collection,” *Small* **11**(34), 4379–4384 (2015).
- K. C. Park, S. S. Chhatre, S. Srinivasan, R. E. Cohen, and G. H. McKinley, “Optimal design of permeable fiber network structures for fog harvesting,” *Langmuir* **29**(43), 13269–13277 (2013).
- R. Labbé and C. Duprat, “Capturing aerosol droplets with fibers,” *Soft Matter* **15**(35), 6946–6951 (2019).
- A. Moncuquet, A. Mitranescu, O. C. Marchand, S. Ramanarivo, and C. Duprat, “Collecting fog with vertical fibres: Combined laboratory and in-situ study,” *Atmos. Res.* **277**, 106312 (2022).
- P. B. Bintein, A. Cornu, F. Weyer, N. De Coster, N. Vandewalle, and D. Terwagne, “Kirigami fog nets: How strips improve water collection,” *Npj Clean Water* **6**(1), 54 (2023).
- R. Rioboo, M. Marengo, and C. Tropea, “Outcomes from a drop impact on solid surfaces,” *At. Sprays* **11**, 155–165 (2001).
- A. L. Yarín, “Drop impact dynamics: Splashing, spreading, receding, bouncing,” *Annu. Rev. Fluid Mech.* **38**, 159–192 (2006).
- M. Marengo, C. Antonini, I. V. Roisman, and C. Tropea, “Drop collisions with simple and complex surfaces,” *Curr. Opin. Colloid Interface Sci.* **16**, 292–302 (2011).
- C. Josserand and S. T. Thoroddsen, “Drop impact on a solid surface,” *Annu. Rev. Fluid Mech.* **48**, 365–391 (2016).
- J. Breitenbach, I. V. Roisman, and C. Tropea, “From drop impact physics to spray cooling models: A critical review,” *Exp. Fluids* **59**, 55 (2018).
- L. Xu, W. W. Zhang, and S. R. Nagel, “Drop splashing on a dry smooth surface,” *Phys. Rev. Lett.* **94**, 184505 (2005).
- J. C. Fernández-Toledano, B. Braeckveldt, M. Marengo, and J. De Coninck, “How wettability controls nanoprinting,” *Phys. Rev. Lett.* **124**(22), 224503 (2020).
- M. Broom and G. R. Willmott, “Water drop impacts on regular micropillar arrays: Asymmetric spreading,” *Phys. Fluids* **35**, 077120 (2023).
- É. Lorenceau and D. Quéré, “Drops impacting a sieve,” *J. Colloid Interface Sci.* **263**(1), 244–249 (2003).
- D. Bartolo, F. Bouamrène, É. Verneuil, A. Buguin, P. Silberzan, and S. Moulinet, “Bouncing or sticky droplets: Impalement transitions on superhydrophobic micropatterned surfaces,” *Europhys. Lett.* **74**(2), 299–305 (2006).
- D. Soto, H. L. Girard, A. Le Helloco, T. Binder, D. Quéré, and K. K. Varanasi, “Droplet fragmentation using a mesh,” *Phys. Rev. Fluids* **3**, 083602 (2018).
- M. Abouelsoud, A. Kherbeche, and M. J. Thoraval, “Drop impact on a mesh—Viscosity effect,” *J. Colloid Interface Sci.* **648**, 37–45 (2023).
- A. A. Mehrizi, L. Sun, Z. Jun, B. Pang *et al.*, “Droplet impact dynamics on a flexible superhydrophobic cantilever wire mesh,” *Surf. Interfaces* **44**, 103736 (2024).
- C. Boscariol, S. Chandra, D. Sarker, C. Crua, and M. Marengo, “Drop impact onto attached metallic meshes: Liquid penetration and spreading,” *Exp. Fluids* **59**(12), 189 (2018).
- A. Kumar, A. Tripathy, Y. Nam, C. Lee, and P. Sen, “Effect of geometrical parameters on rebound of impacting droplets on leaky superhydrophobic meshes,” *Soft Matter* **14**(9), 1571–1580 (2018).
- Y. Zong, A. Oron, H. Liu, and Y. Jiang, “Dynamic and quasi-static droplet penetration through meshes,” *Langmuir* **39**(28), 9808–9815 (2023).
- L. Xu, W. Ji, J. Lu, Y. Li, J. Hao, G. Hu, and J. M. Floryan, “Droplet impact on a prewetted mesh,” *Phys. Rev. Fluids* **6**, L101602 (2021).
- R. Rioboo, M. Marengo, and C. Tropea, “Time evolution of liquid drop impact onto solid, dry surfaces,” *Exp. Fluids* **33**, 112–124 (2002).
- G. Zhang, M. A. Quetzeri-Santiago, C. A. Stone, L. Botto, and J. R. Castrejón-Pita, “Droplet impact dynamics on textiles,” *Soft Matter* **14**(40), 8182–8190 (2018).
- C. Lee, Y. Nam, H. Lastakowski, J. I. Hur, S. Shin, A. L. Bianco, C. Pirat, C. J. Kim, and C. Ybert, “Two types of Cassie-to-Wenzel wetting transitions on superhydrophobic surfaces during drop impact,” *Soft Matter* **11**(23), 4592–4599 (2015).



- <sup>27</sup>S. Ryu, P. Sen, Y. Nam, and C. Lee, "Water penetration through a superhydrophobic mesh during a drop impact," *Phys. Rev. Lett.* **118**, 014501 (2017).
- <sup>28</sup>K. Vontas, C. Boscariol, M. Andreadaki, A. Georgoulas, C. Crua, J. H. Walther, and M. Marengo, "Droplet impact on suspended metallic meshes: Effects of wettability, Reynolds and Weber numbers," *Fluids* **5**, 81 (2020).
- <sup>29</sup>A. A. Mehrizi, S. Lin, L. Sun, Y. Wang, and L. Chen, "Penetration and ligament formation of viscoelastic droplets impacting on the superhydrophobic mesh," *Sci. Rep.* **12**, 11920 (2022).
- <sup>30</sup>A. A. Mehrizi, S. Lin, L. Sun, and L. Chen, "Spectacular behavior of a viscoelastic droplet impinging on a superhydrophobic mesh," *Langmuir* **38**, 6106–6115 (2022).
- <sup>31</sup>U. Sen, T. Roy, S. Chatterjee, R. Ganguly, and C. M. Megaridis, "Post-impact behavior of a droplet impacting on a permeable metal mesh with a sharp wettability step," *Langmuir* **35**, 12711 (2019).
- <sup>32</sup>L. Xu, S. Zong, J. Hao, and J. M. Floryan, "Droplet penetration through an inclined mesh," *Phys. Fluids* **34**, 122105 (2022).
- <sup>33</sup>D. Richard, C. Clanet, and D. Quéré, "Contact time of a bouncing drop," *Nature* **417**, 811 (2002).
- <sup>34</sup>D. Song, X. Liu, X. Wang, X. Du, and H. Hu, "Experimental investigation on the droplet stability of superhydrophobic mesh," *Coatings* **13**, 756 (2023).
- <sup>35</sup>C. D. Modak, A. Kumar, A. Tripathy, and P. Sen, "Drop impact printing," *Nat. Commun.* **11**, 4327 (2020).
- <sup>36</sup>S. Catsoulis, U. Sen, J. H. Walther, and C. M. Megaridis, "Droplet impact on a wettability-patterned woven mesh," *Droplet* **2**, e53 (2023).
- <sup>37</sup>G. Wang, J. Gao, and K. H. Luo, "Droplet impacting a superhydrophobic mesh array: Effect of liquid properties," *Phys. Rev. Fluids* **5**(12), 123605 (2020).
- <sup>38</sup>J. L. Wilson, A. A. Pahlavan, M. A. Erinin, C. Duprat, L. Deike, and H. A. Stone, "Aerodynamic interactions of drops on parallel fibres," *Nat. Phys.* **19**(11), 1667–1672 (2023).
- <sup>39</sup>R. Akbari, G. Ramos Chagas, G. Godeau, M. Mohammadzadeh, F. Guittard, and T. Darmanin, "Intrinsically water-repellent copper oxide surfaces; An electro-crystallization approach," *Appl. Surf. Sci.* **443**, 191–197 (2018).
- <sup>40</sup>R. Akbari, G. Godeau, M. Mohammadzadeh, F. Guittard, and T. Darmanin, "Wetting transition from hydrophilic to superhydrophobic over dendrite copper leaves grown on steel meshes," *J. Bionic Eng.* **16**(4), 719–729 (2019).
- <sup>41</sup>R. Akbari, M. R. Mohammadzadeh, C. Antonini, F. Guittard, and T. Darmanin, "Controlling morphology and wettability of intrinsically superhydrophobic copper-based surfaces by electrodeposition," *Coatings* **12**, 1260 (2022).
- <sup>42</sup>T. Maitra, C. Antonini, M. Auf Der Mauer, C. Stamatopoulos, M. K. Tiwari, and D. Poulikakos, "Hierarchically nanotextured surfaces maintaining superhydrophobicity under severely adverse conditions," *Nanoscale* **6**(15), 8710–8719 (2014).
- <sup>43</sup>I. S. Khattab, F. Bandarkar, M. A. A. Fakhree, and A. Jouyban, "Density, viscosity, and surface tension of water+ethanol mixtures from 293 to 323K," *Korean J. Chem. Eng.* **29**(6), 812–817 (2012).
- <sup>44</sup>R. Akbari and C. Antonini, "Contact angle measurements: From existing methods to an open-source tool," *Adv. Colloid Interface Sci.* **294**, 102470 (2021).
- <sup>45</sup>W. Li and A. Amirfazli, "A thermodynamic approach for determining the contact angle hysteresis for superhydrophobic surfaces," *J. Colloid Interface Sci.* **292**(1), 195–201 (2005).
- <sup>46</sup>R. Rioboo, B. Delattre, D. Duvivier, A. Vaillant, and J. De Coninck, "Superhydrophobicity and liquid repellency of solutions on polypropylene," *Adv. Colloid Interface Sci.* **175**, 1–10 (2012).
- <sup>47</sup>C. Antonini, F. Villa, I. Bernagozzi, A. Amirfazli, and M. Marengo, "Drop rebound after impact: The role of the receding contact angle," *Langmuir* **29**(52), 16045–16050 (2013).
- <sup>48</sup>M. Reyssat, A. Pépin, F. Marty, Y. Chen, and D. Quéré, "Bouncing transitions on microtextured materials," *Europhys. Lett.* **74**(2), 306–312 (2006).
- <sup>49</sup>Y. C. Jung and B. Bhushan, "Dynamic effects of bouncing water droplets on superhydrophobic surfaces," *Langmuir* **24**(12), 6262–6269 (2008).
- <sup>50</sup>T. Maitra, C. Antonini, M. K. Tiwari, A. Mularczyk, Z. Imeri, P. Schoch, and D. Poulikakos, "Supercooled water drops impacting superhydrophobic textures," *Langmuir* **30**, 10855–10861 (2014).
- <sup>51</sup>A. N. L. K. Malla, N. D. Patil, and R. Bhardwaj, "Droplet bouncing and breakup during impact on a microgrooved surface," *Langmuir* **33**, 9620–9631 (2017).
- <sup>52</sup>A. Hu and D. Liu, "3D simulation of micro droplet impact on the structured superhydrophobic surface," *Int. J. Multiphase Flow* **147**, 103887 (2022).
- <sup>53</sup>B. X. Zhang, Z. H. Cai, Q. Ding, K. Q. Zhu, Y. R. Yang, and X. D. Wang, "Bouncing dynamics of nanodroplets impacting superhydrophobic surfaces: The coupling influence of wetting transitions and scale effects," *Colloids Surf., A* **657**, 130579 (2023).
- <sup>54</sup>F. Wang and T. Fang, "Retraction dynamics of water droplets after impacting upon solid surfaces from hydrophilic to superhydrophobic," *Phys. Rev. Fluids* **5**, 033604 (2020).
- <sup>55</sup>P. Brunet, F. Lapiere, F. Zoueshtiagh, V. Thomy, and A. Merlen, "To grate a liquid into tiny droplets by its impact on a hydrophobic microgrid," *Appl. Phys. Lett.* **95**, 254102 (2009).
- <sup>56</sup>E. Klaseboer, R. Manica, and D. Y. C. Chan, "Universal behavior of the initial stage of drop impact," *Phys. Rev. Lett.* **113**, 194501 (2014).
- <sup>57</sup>B. Zhang, V. Sanjay, S. Shi, Y. Zhao, C. Lv, X.-Q. Feng, and D. Lohse, "Impact forces of water drops falling on superhydrophobic surfaces," *Phys. Rev. Lett.* **129**, 104501 (2022).
- <sup>58</sup>M. V. Chubynsky, K. I. Belousov, D. A. Lockerby, and J. E. Sprittles, "Bouncing off the Walls: The influence of gas-kinetic and van der Waals effects in drop impact," *Phys. Rev. Lett.* **124**, 084501 (2020).
- <sup>59</sup>J. Xu, J. Xie, X. He, Y. Cheng, and Q. Liu, "Water drop impacts on a single-layer of mesh screen membrane: Effect of water hammer pressure and advancing contact angles," *Exp. Therm. Fluid Sci.* **82**, 83–93 (2017).
- <sup>60</sup>W. Liwei, W. Xiao, Y. Weijie, H. Pengfei, H. Feng, and Z. Xiwen, "Numerical study of droplet fragmentation during impact on mesh screens," *Microfluid. Nanofluid.* **23**, 136 (2019).
- <sup>61</sup>M. J. Su, Y. Luo, G. W. Chu, Y. Cai, Y. Le, L. L. Zhang, and J. F. Chen, "Dispersion behaviors of droplet impacting on wire mesh and process intensification by surface micro/nano-structure," *Chem. Eng. Sci.* **219**, 115593 (2020).
- <sup>62</sup>C. Clanet, C. Béguin, D. Richard, and D. Quéré, "Maximal deformation of an impacting drop," *J. Fluid Mech.* **517**, 199–208 (2004).
- <sup>63</sup>M. J. Wang, Y. L. Hung, F. H. Lin, and S. Y. Lin, "Dynamic behaviors of droplet impact and spreading: A universal relationship study of dimensionless wetting diameter and droplet height," *Exp. Therm. Fluid Sci.* **33**, 1112–1118 (2009).
- <sup>64</sup>C. Antonini, A. Amirfazli, and M. Marengo, "Drop impact and wettability: From hydrophilic to superhydrophobic surfaces," *Phys. Fluids* **24**, 102104 (2012).
- <sup>65</sup>Y. Wei and M. J. Thoraval, "Maximum spreading of an impacting air-in-liquid compound drop," *Phys. Fluids* **33**, 061703 (2021).
- <sup>66</sup>Y. Liu, L. Moevius, X. Xu, T. Qian, J. M. Yeomans, and Z. Wang, "Pancake bouncing on superhydrophobic surfaces," *Nat. Phys.* **10**, 515–519 (2014).